catalysts

MDPI

Article

Ordered Mesoporous $MnAlO_x$ Oxides Dominated by Calcination Temperature for the Selective Catalytic Reduction of NO_x with NH_3 at Low Temperature

Qixiong Hou [1], Yongjin Liu [1,2], Yaqin Hou [1,*], Xiaojin Han [1] and Zhanggen Huang [1,2,*]

[1] State Key Laboratory of Coal Conversion, Institute of Coal Chemistry, Chinese Academy of Sciences, Taiyuan 030001, China; houqixiong@163.com (Q.H.); ucasliuyongjin@163.com (Y.L.); hanxiaojin@sxicc.ac.cn (X.H.)
[2] University of Chinese Academy of Sciences, Beijing 100049, China
* Correspondence: houyaqin@sxicc.ac.cn (Y.H.); zghuang@sxicc.ac.cn (Z.H.)

Abstract: Manganese alumina composited oxides ($MnAlO_x$) catalysts with ordered mesoporous structure prepared by evaporation-induced self-assembly (EISA) method was designed for the selective catalytic reduction (SCR) of NO_x with NH_3 at low temperature. The effect of calcination temperature of $MnAlO_x$ catalysts was investigated systematically, and it was correlated with SCR activity. Results showed that with an increase in calcination temperature, the SCR activity of $MnAlO_x$ catalysts increased. When the calcination temperature was raised up to 800 °C, the NO_x conversion was more than 90% in the operation temperature range of 150~240 °C. Through various characterization analysis, it was found that $MnAlO_x$-800 °C catalysts possessed enhanced redox capacities as the higher content of $Mn^{4+}/(Mn^{3+} + Mn^{4+})$. Moreover, the improved redox properties could contribute to a higher NO_x adsorption and activation ability, which lead to higher SCR performance of $MnAlO_x$-800 °C catalysts. In situ DRIFTs revealed that the adsorbed NO_2 and bidentate nitrate are the reactive intermediate species, and NH_3 species bonded to Lewis acid sites taken part in SCR progress. The SCR progress predominantly followed E–R mechanism, while L–H mechanism also takes effect to a certain degree.

Keywords: ordered mesoporous $MnAlO_x$; calcination temperature; SCR; low temperature

Citation: Hou, Q.; Liu, Y.; Hou, Y.; Han, X.; Huang, Z. Ordered Mesoporous $MnAlO_x$ Oxides Dominated by Calcination Temperature for the Selective Catalytic Reduction of NO_x with NH_3 at Low Temperature. *Catalysts* **2022**, *12*, 637. https://doi.org/10.3390/catal12060637

Academic Editor: Rufino M. Navarro Yerga

Received: 11 May 2022
Accepted: 6 June 2022
Published: 10 June 2022

1. Introduction

Emission of nitrogen oxides (NO_x) from the burning of fossil fuel, including the stationary and mobile source, are regarded as the major source of atmospheric contamination. They have brought about a series of serious healthcare and environmental issues, such as fine particle pollution, acid rain, photochemical smog, and ozone depletion [1–3]. Great efforts have been devoted to alleviating the emission of NO_x to meet the increasingly strict emission legislation and policies enacted by government. Selective catalytic reduction of NO_x with NH_3 (NH_3-SCR) is well-established as the most effective technology for the abatement of NO_x [4].

Many kinds of SCR catalysts have been extensively reported, among which V_2O_5-WO_3/TiO_2 catalysts are the most worldwide used and effective commercial catalyst on account of the admirable catalytic activity in a working temperature range of 300~400 °C [5,6]. However, this kind of SCR catalyst has some non-negligible drawbacks in practical application, such as the toxicity of V_2O_5, narrow working temperature window, the generation of N_2O at high temperature, and particularly the poor activity at low temperature [7–9]. Simultaneously, the SCR system has always placed the dust precipitation and desulfurization unit upstream, and the catalysts inevitably suffered the serious deactivation from dust accumulation on the catalyst surface and the chemical poisoning of SO_2 [10]. Therefore, a

tail-end installation and development of an appropriate SCR catalyst with high activity at low working temperature (<250 °C) is significant for industrial applications.

Some transition metal oxides (e.g., MnO_x, FeO_x, CoO_x, CuO_x, CeO_x) catalysts have been extensively studied in the low temperature NH_3-SCR reaction. Among these, manganese-based catalysts demonstrated high SCR catalytic activity since they possess various kinds of labile surface oxygen, which are significant to accomplish the catalytic cycle [11,12]. In order to enhance the acidic/redox properties of pure MnO_x catalysts, supported MnO_x multiple oxides catalysts are extensively investigated due to the improvement of the dispersion of MnO_x, the strong metal–support interaction, and promotion of the electron transfer between active constituents. MnO_x supported on Al_2O_3 [13,14], TiO_2 [12,15,16], and carbon materials [17–19] for NH_3-SCR reaction have been intensively studied. According to the previous investigations, MnO_x with amorphous phase demonstrated higher SCR activity at low temperature in comparison with highly crystallized ones [20–22]. It is known from previous literatures that the high dispersion of MnO_x contributes to generate amorphous phase [20].

However, most of the MnO_x/Al_2O_3 catalysts afore mentioned are prepared by the conventional impregnation method, which cannot guarantee that MnO_x dispersed on the surface of the Al_2O_3 support homogeneously and tend to agglomerate during the process of catalytic reaction. Wu et al. reported MnO_x/TiO_2 catalysts prepared by three methods for SCR at low temperature [23]. The SCR activity of MnO_x/TiO_2 increased in the following sequence: coprecipitation < impregnation < sol–gel. MnO_x/TiO_2 catalysts prepared by sol–gel method demonstrated higher dispersion of active components, lower crystallinity, and stronger interaction than other two catalysts. Compared to the Mn-Fe/TiO_2 catalysts prepared by an impregnation method, the catalysts prepared by a deposition–precipitation exhibited higher catalytic activity at low temperature. The deposition–precipitation method facilitated to the amorphous active components, enhanced the surface area, surface labile oxygen, acidity, and acid strength while promoting the reduction of active components [24]. Hence, it is deduced that the preparation method has a terrific effect on the dispersion and structure of the active species, as well as the interaction between the active constituents. Therefore, it is worth exploring more effective preparation methods to enhance the NH_3-SCR activity.

Ordered mesoporous alumina (OMA) supported metal oxides have emerged as a new group of functional materials with enhanced catalytic activity and selectivity. In comparison to the wet impregnation of OMA with metal oxide precursors, which often leads to structure blockage and/or damage, the evaporation-induced self-assembly (EISA) synthesis of OMA-supported metal oxides is suitable to achieve high-quality mesostructure that exhibit strong metal–support interactions and retain homogeneous distribution of active sites [25,26]. Hence, we assume that the EISA method might a promising way to obtain high dispersion of MnO_x on the surface of Al_2O_3 and these catalysts would exhibit high SCR activity at low temperature. However, MnO_x/Al_2O_3 catalysts prepared by EISA method for SCR reaction have rarely been investigated. Besides, owning to the SCR reaction being an exothermic process, the fluctuation of heat is bound to have an impact on the structure and reaction activity of the catalyst. Hence, it is very imperative to investigate the influence of the calcination temperature on the catalytic performance of the catalysts.

In this paper, MnO_x/Al_2O_3 catalysts prepared by EISA method with different calcination temperature were applied to the NH_3-SCR at low temperature. The SCR performance of the $MnAlO_x$ catalysts with different calcination temperature were compared and discussed. To illuminate the outstanding performance of $MnAlO_x$-800 °C, the physicochemical characters of the $MnAlO_x$ catalysts were investigated by multifarious characterization methods. Simultaneously, the reaction mechanism was investigated by using in situ DRIFTs. The main objective of our present work is not only to optimize the calcination temperature of the $MnAlO_x$ catalysts prepared by EISA method, but more significantly, it seeks to elucidate the structural–performance correlation of the catalyst.

2. Results and Discussion

2.1. NO_x Conversion and N_2 Selectivity

Figure 1 shows that the NH_3-SCR performances over $MnAlO_x$-T catalysts calcined at different temperatures. As shown in Figure 1, the NO_x conversion of $MnAlO_x$-T catalysts increased with raising the reaction temperature in the temperature range of 90~240 °C. It could be observed that the $MnAlO_x$-450 °C and $MnAlO_x$-550 °C catalysts exhibited a similar catalytic activity throughout the whole temperature range. In contrast, the $MnAlO_x$-800 °C shows exceptional activity, and the NO_x conversion was more than 90% in the range of 150~240 °C.

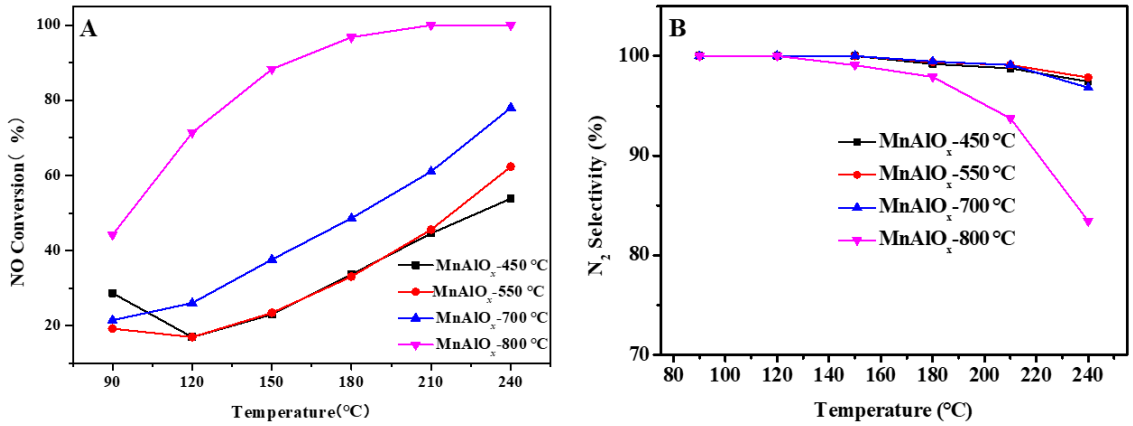

Figure 1. (**A**) The NO_x conversion and (**B**) N_2 selectivity of $MnAlO_x$ catalysts.

As shown in Figure 1B, the N_2 selectivity of $MnAlO_x$-T catalysts decreased with raising the reaction temperature due to the unselective oxidation of NH_3 by O_2 into N_2O. It is noted that there is only a few ppm of N_2O detected over $MnAlO_x$-T (T = 450, 550, 700 °C) catalysts in the temperature range of 90~240 °C, which makes a major contribution to the excellent N_2 selectivity with more than 96% even at 240 °C. The N_2 selectivity of $MnAlO_x$-800 °C decreases remarkably with the increase reaction temperature, and $MnAlO_x$-800 °C demonstrates an excellent N_2 selectivity with more than 82%, even at 240 °C.

2.2. Textural and Structural Properties

2.2.1. BET

First, we determined the calcination temperature of $MnAlO_x$ samples on the basis of TG-DTG analysis (Supporting Information in Figure S1). To investigate the texture and porosity of mesoporous $MnAlO_x$-T catalysts, we characterized the catalysts using N_2 adsorption/desorption isotherm analysis. The N_2 adsorption/desorption isotherms and the corresponding pore size distribution (PSD) of mesoporous $MnAlO_x$ catalysts are shown in Figure 2. It is suggested that the adsorption/desorption isotherms of $MnAlO_x$-T catalysts all yield type IV isotherms, suggesting the presence of mesopores according to the definition of IUPAC [27]. All the isotherms were type H1-shaped hysteresis loops in the relative pressure from 0.5 to 0.95, indicating that these structures highly ordered cylindrical mesoporous channels, which were in accordant with TEM results. In the Type H1 hysteresis loops, the two branches are almost vertical and nearly parallel over an appreciable range of gas uptake. Type H1 is often associated with porous materials known, from other evidence, to consist of agglomerates or compacts of approximately uniform spheres in properly regular array, and hence to have narrow distribution of pore size. The steepness of the capillary condensation step indicates uniformity of mesopores. The corresponding PSD curves in Figure 2B are in accordance with the adsorption isotherms in Figure 2A. As depicted in Figure 2B, the PSD curves of these mesoporous material were mainly focused on 8.0 nm, indicating that the PSD of all the samples was uniform relatively. Meanwhile, narrow pore size distribution is maintained though the calcination temperature increases.

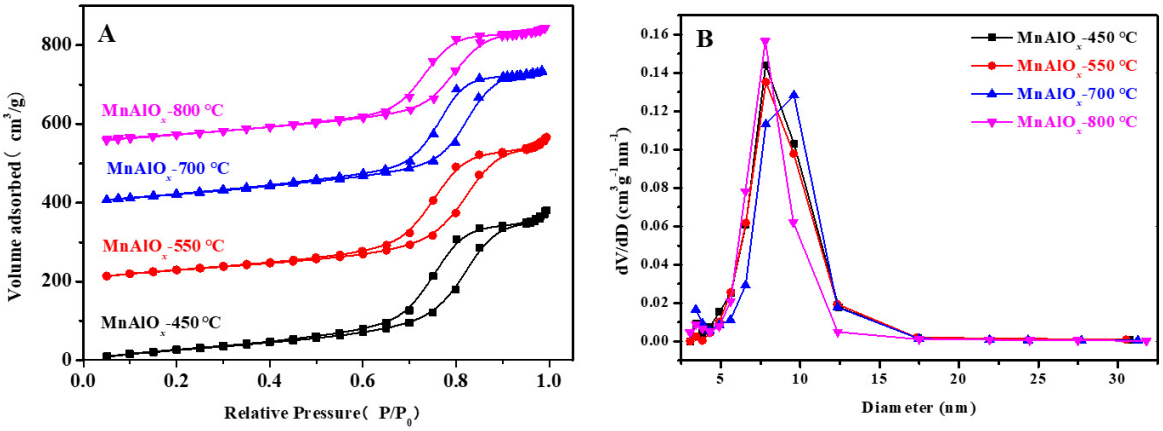

Figure 2. (**A**) N_2 adsorption/desorption isotherm and (**B**) the corresponding pore size distribution for mesoporous $MnAlO_x$ catalysts with different calcined temperature.

The structural parameters derived from these isotherms are summarized in Table 1. As shown in Table 1, it was found that the surface area of mesoporous $MnAlO_x$-450 °C was 247.7 m^2/g, which was larger comparing to these of mesoporous $MnAlO_x$-550 °C (221.3 m^2/g), $MnAlO_x$-700 °C (226.5 m^2/g), and $MnAlO_x$-800 °C (196.2 m^2/g) catalysts. Although the surface area of $MnAlO_x$ catalysts prepared at a low calcination temperature is higher than that prepared at a high calcination temperature, the SCR activity over later is still higher than that over the former (Figure 1), which signifies that the SCR activity over these catalysts is not only related with the surface area, but also related with some other structural or redox properties, which will be discussed later in this paper.

Table 1. BET surface area and NH_3 storage of $MnAlO_x$-T catalysts.

Samples	S_{BET}	V_{pore}	Diameter	NH_3 Storage
	m^2/g	cm^3/g	nm	mmol/g
$MnAlO_x$-450 °C	247.7	0.661	10.683	1.692
$MnAlO_x$-550 °C	221.3	0.621	11.222	1.470
$MnAlO_x$-700 °C	226.5	0.584	10.312	0.994
$MnAlO_x$-800 °C	196.2	0.501	10.220	0.795

2.2.2. Small-Angle XRD and TEM

Proof of the appearance of ordered mesostructure for the $MnAlO_x$ samples is afforded by the small angle XRD patterns (Figure 3) and TEM images (Figure 4). It is well-known that the small angle X-ray diffraction patterns provide information about the possible organization of mesopores [25,28]. As illustrated in Figure 3, very strong diffraction peaks of (110) plane around 0.8° and a weak and overlapped diffraction peaks of (110) and (200) plane around 1.7° for mesoporous $MnAlO_x$ were observed, which suggested the formation of ordered mesoporous structure. Therefore, the small-angle XRD patterns indicate the presence of uniform mesoporous.

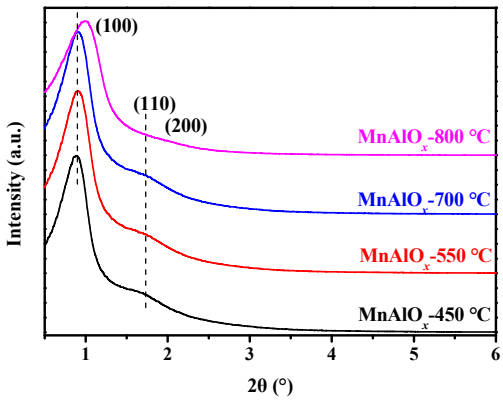

Figure 3. Small-angle patterns of mesoporous MnAlO$_x$-T catalysts.

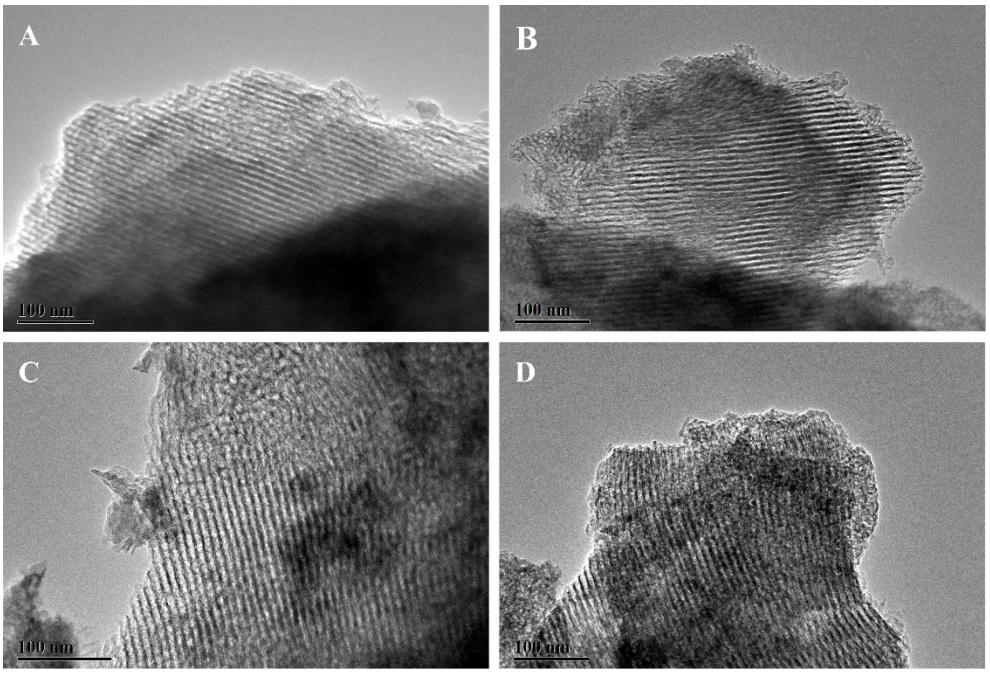

Figure 4. TEM images of (**A**) MnAlO$_x$-450 °C, (**B**) MnAlO$_x$-550 °C, (**C**) MnAlO$_x$-700 °C, (**D**) MnAlO$_x$-800 °C.

The morphology and structure of MnAlO$_x$ catalysts were investigated by TEM, the results are illustrated in Figure 4. The TEM images of MnAlO$_x$ samples show the presence of domains with ordered channel-like mesopores, which is in good agreement with the XRD patterns at small angles. The TEM images also show that the channels are uniform, which corresponds to the pore diameter obtained from the adsorption/desorption isotherms illustrated in Figure 2B. Therefore, on the basis of the BET, small angle XRD, and TEM results, MnAlO$_x$ samples with uniform and ordered mesopores were successfully prepared by EISA method.

2.2.3. Wide-Angle XRD and SEM

Wide-angle XRD patterns of mesoporous MnAlO$_x$ catalysts results were depicted in Figure 5. The diffraction peaks of all MnAlO$_x$ catalysts are a weak and broad peak, indicating a poor crystallinity of MnAlO$_x$ catalysts. MnAlO$_x$ catalysts calcined at 800 °C begin to display crystallinity, as supported by the powder XRD patterns with distinctive peaks. Calcination at 450 °C gives rise to the mesostructure with amorphous wall, and then the amorphous wall is converted to γ-Al_2O_3 phase (JCPDS No. 10-0425) after further treatment at a temperature of 800 °C. Furthermore, the diffraction peaks assigned to MnO$_x$

cannot be detected, indicating that the active components (MnO_x) were evenly distributed on the Al_2O_3 surface. Furthermore, we characterized the element dispersion of the $MnAlO_x$ catalysts via SEM-EDS measurements.

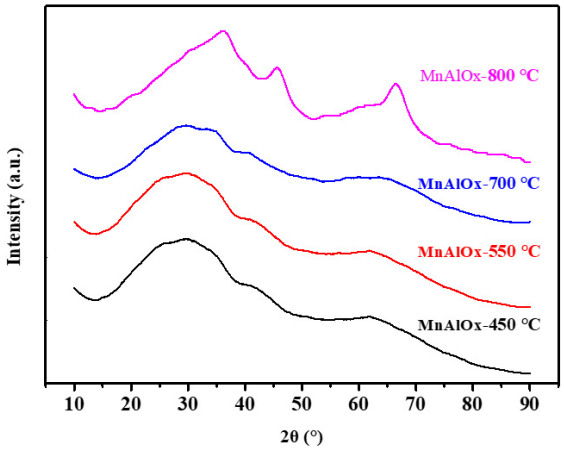

Figure 5. Wide-angle XRD patterns of mesoporous $MnAlO_x$ catalysts.

The SEM-EDS measurements were further conducted to determine the elemental constituents of the $MnAlO_x$ samples, and the results are illustrated in Figure 6. The homogeneous distribution of the elements within the framework of $MnAlO_x$ samples was confirmed by the density of the Mn, O, and Al spots in the elements mapping. The SEM-EDS measurements indicate a homogeneous distribution of Mn, Al, and O species throughout the entire periodic mesostructure (mixed oxides phase) instead of isolated single oxide domains, which is consistent with the wide angle XRD results. Thus, the atomic-level homogeneity of the OMA-supported metal oxides framework was clearly achieved by EISA method.

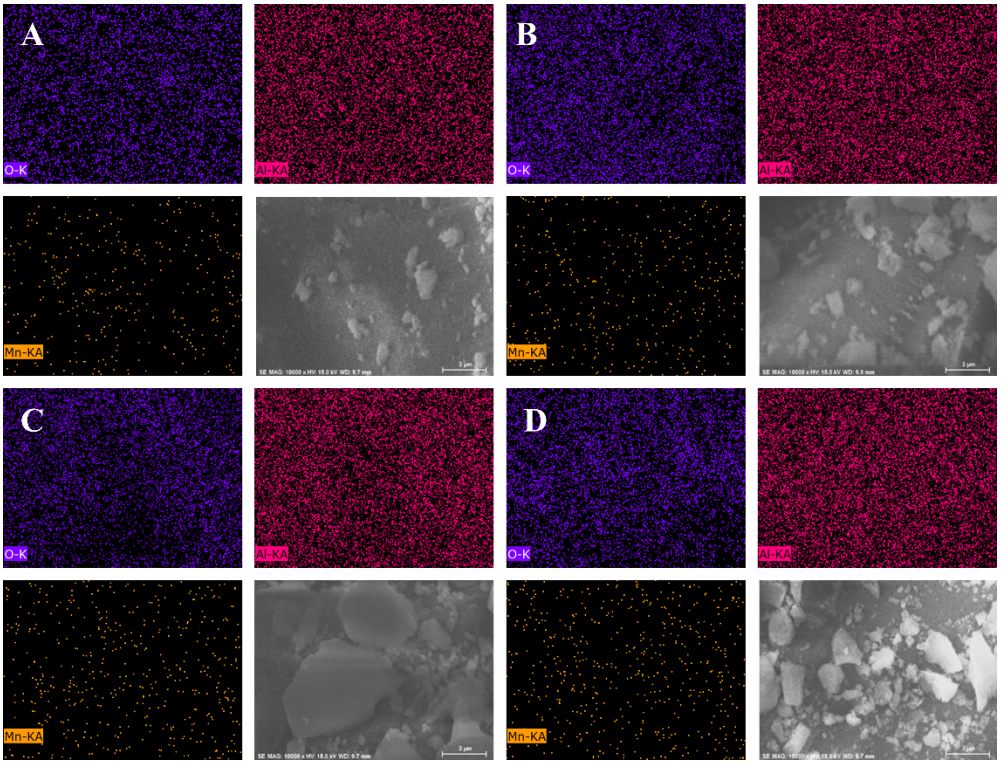

Figure 6. SEM-EDS images of (**A**) $MnAlO_x$-450 °C, (**B**) $MnAlO_x$-550 °C, (**C**) $MnAlO_x$-700 °C, (**D**) $MnAlO_x$-800 °C.

2.3. Adsorption/Desorption Properties

2.3.1. NH_3-TPD

The acidity of SCR catalyst is crucial for the catalytic activity because it is responsible for the adsorption and activation of NH_3. Herein, NH_3-TPD was performed to investigate the strength of acid sites and the surface acid amount of the catalysts, and the results are demonstrated in Figure 7. All $MnAlO_x$ catalysts exhibit two desorption peaks: the low temperature desorption peaks around at 144 °C attributed to the NH_3 desorbed by weak acid sites, and the high-temperature desorption peak around at 524 °C assigned to strong acid sites on the catalysts. Because the NH_3 molecules coordinated to the Lewis acid sites exhibit higher thermal stability than the NH_4^+ ions bounded to the Brønsted acid sites, it can be deduced that the low temperature peak is assigned to NH_4^+ ions bound to the Brønsted acid sites, and the desorption high-temperature peaks are associated with coordinated NH_3 molecular originating from the Lewis acid sites [29]. Moreover, it is well known that the area and position of desorption peak are correlated with the acid concentration and acid strength, respectively. In addition, the NH_3-TPD profile of $MnAlO_x$ catalysts calcined at low temperature reveals the much larger area, indicating the presence of abundant acid sites due to its larger surface area. Although the NH_3 adsorption capacity of $MnAlO_x$ catalysts prepared at a low calcination temperature is much higher than that prepared at a high calcination temperature, the SCR activity over the latter is still a little higher than that over the former, as shown in Figure 1, which implies that the SCR activity over these catalysts is not only related with the NH_3 adsorption capacity, but also related with some other structural or redox properties, which will be discussed in detail later.

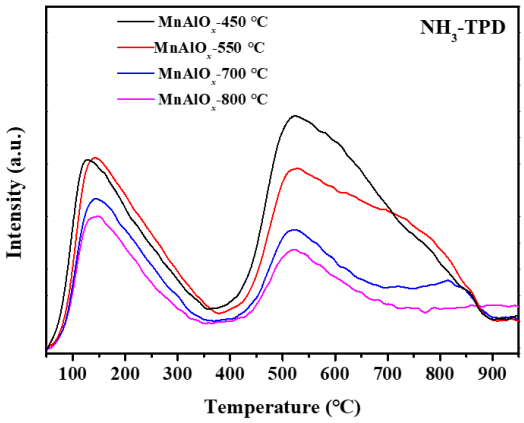

Figure 7. NH_3-TPD profiles of the $MnAlO_x$ catalysts.

2.3.2. NO + O_2-TPD

The variation of the NO_x concentration during the desorption process as a function of the temperature is illustrated in Figure 8. It is evidenced that there are three groups of NO_x desorption peaks detected over $MnAlO_x$ serials catalysts. In comparison with the in situ DRIFTs spectra of NO + O_2 co-adsorption on $MnAlO_x$ catalysts at different temperature (which would be further discussed in Section 2.5), among which the peak at 133 °C is ascribed to the decomposition of the adsorbed NO_2, and the peak at 189 °C is assigned to the decomposition of the bridging nitrate, linear nitrite and monodentate nitrite according to the DRIFTs result of NO + O_2 co-adsorption. The band located at 331 °C is attributed to the decomposition of the bidentate nitrate, since bidentate nitrate usually shows much higher thermal stability [30–33].

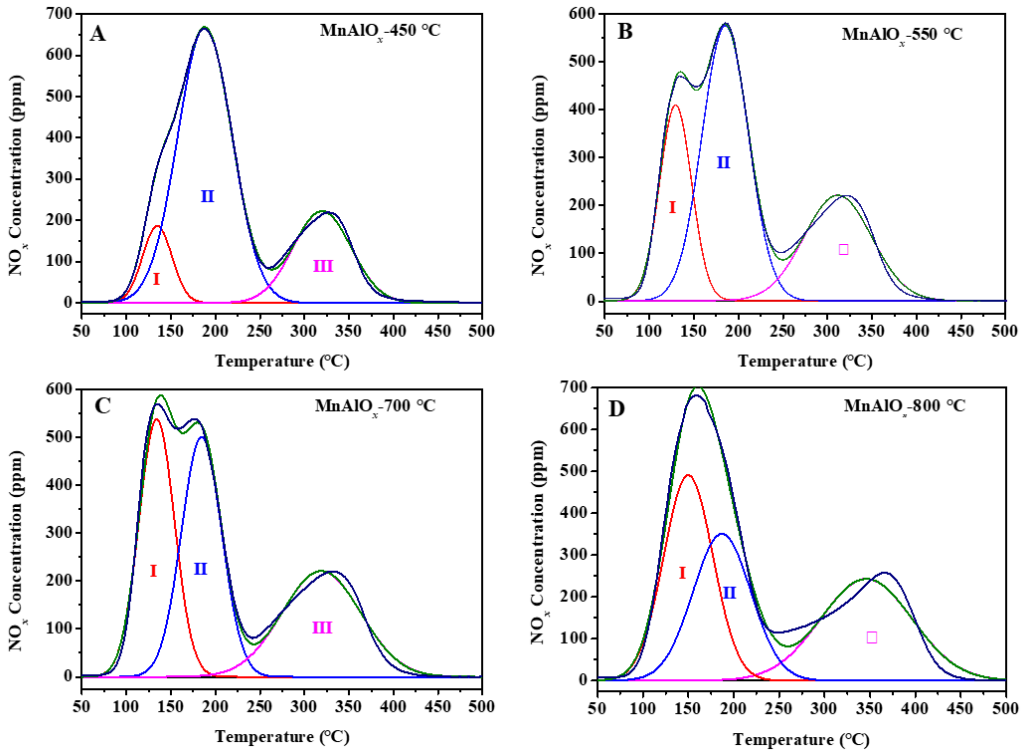

Figure 8. NO + O_2-TPD profiles of (**A**) $MnAlO_x$-450 °C, (**B**) $MnAlO_x$-550 °C, (**C**) $MnAlO_x$-700 °C, (**D**) $MnAlO_x$-800 °C.

The normalized integral areas of the NO_x desorption bands by the surface area depicted in Table 2. It is noticeable that with the increase of the calcination temperature from 450 to 800 °C, the total desorption amount of NO_x over $MnAlO_x$ catalysts increases dramatically. Meanwhile, the desorption amount of adsorbed NO_2 and bidentate nitrate progressively increase and the desorption amount of monodentate nitrite, linear nitrite, and bridged nitrate progressively decrease as the calcination temperature continues increasing. This result means that the high calcination temperature results in the enhancement of NO oxidation to NO_2 and the improvement of the adsorption of NO_x as nitrate species. Compared with these $MnAlO_x$ catalysts, more NO_x-intermediates species on the $MnAlO_x$ catalyst surface calcined at high temperatures could participate in the SCR reaction, which is beneficial to promoting the SCR activity.

Table 2. Capacities of $MnAlO_x$ catalysts for NO_x adsorption.

Samples	NO_x Storage mmol/g	Peak I	Peak II	Peak III
		Adsorbed NO_2	Monodentate Nitrite Linear Nitrite Bridged Nitrate	Bidentate Nitrate
$MnAlO_x$-450 °C	0.1372	0.0138	0.0911	0.0323
$MnAlO_x$-550 °C	0.1366	0.0327	0.0666	0.0373
$MnAlO_x$-700 °C	0.1414	0.0478	0.0503	0.0434
$MnAlO_x$-800 °C	0.1623	0.0588	0.0494	0.0541

2.4. Redox Capability

According to SCR reaction mechanism [2], the excellent reducibility and strong acidity are two crucial factors for rendering a catalyst with an admirable SCR performance at a broad temperature range, which are responsible for the adsorption/activation of NH_3 and NO_x. The redox behaviors of $MnAlO_x$ catalysts were investigated simultaneously by H_2-TPR, XPS, and NO oxidation experiments.

2.4.1. H_2-TPR

To discuss the redox behavior of catalysts in this work, the H_2-TPR profiles of different catalysts are shown in Figure 9. Previous studies have demonstrated that the H_2-TPR profile of pristine MnO_x exhibits three reduction peaks at approximately 367, 455, and 517 °C, ascribed to the stepwise reduction of MnO_2 to Mn_2O_3, Mn_2O_3 to Mn_3O_4, Mn_3O_4 to MnO, respectively [34]. All of the H_2-TPR profiles of the $MnAlO_x$ catalysts present two distinct H_2 consumption peaks around 345 and 441 °C, which were attributed to the reduction of MnO_2 to Mn_2O_3, then Mn_2O_3 to Mn_3O_4 with the increased temperature. Compared to the area of the two peaks, it is deduced that the peak ascribed to the reduction of MnO_2 to Mn_2O_3 has a larger area, indicating that MnO_2 is the predominant phase in the catalytic formulations in comparison with Mn_2O_3.

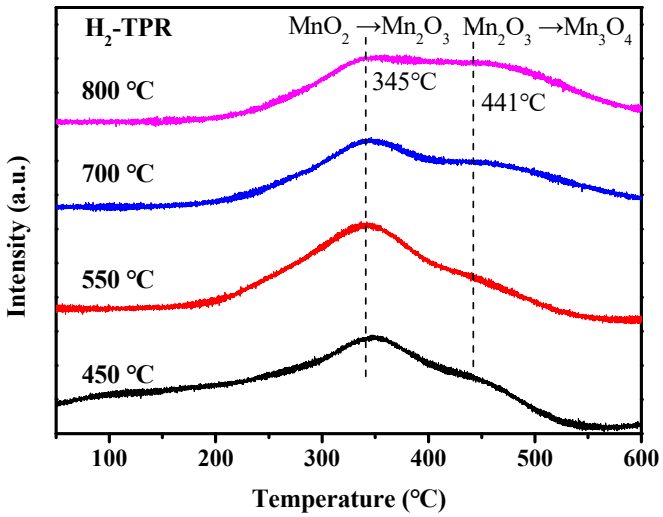

Figure 9. H_2-TPR profiles of different catalysts.

The H_2 consumption of $MnAlO_x$ catalysts calcined at different temperature is quantified and listed in Table 3. Note that the H_2 consumption of $MnAlO_x$ catalysts increased with the increased calcination temperature, indicated that the average oxidation valence states of $MnAlO_x$-800 °C were higher than that of $MnAlO_x$ catalysts calcined at other temperature. This result suggested that the redox capacity of the $MnAlO_x$ serial catalysts enhanced in the following sequence: $MnAlO_x$-800 °C >$MnAlO_x$-700 °C > $MnAlO_x$-550 °C > $MnAlO_x$-450 °C. The higher calcination temperature of $MnAlO_x$ catalysts can enhance the redox capacity, which appears to be responsible for the higher SCR activity of $MnAlO_x$-800 °C catalysts.

Table 3. H_2 consumption amount, surface atomic concentrations of Mn, O, Al, and the relative concentration ratios.

Catalysts	H_2 Consumption Amount mmol/g	Surface Atom Concentrations (%)			Mn^{4+}/Mn^{n+}
		Mn	O	Al	
$MnAlO_x$-450 °C	0.114	2.227	46.27	51.51	49.31
$MnAlO_x$-550 °C	0.132	3.49	39.62	56.89	49.20
$MnAlO_x$-700 °C	0.170	3.78	51.15	45.07	49.03
$MnAlO_x$-800 °C	0.200	6.033	45.26	48.71	51.36

2.4.2. XPS

In order to better understand the Mn species atomic concentration and chemical state on the catalyst surface, XPS analysis of $MnAlO_x$ catalyst with different calcination temperature was carried out. The deconvoluted peaks of Mn 2p are displayed in Figure 10 and the relative concentration ratios of different Mn oxidation states are summarized in Table 3. As shown in Figure 10, two prime peaks assigned to Mn $2p_{3/2}$ and Mn $2p_{1/2}$

of the $MnAlO_x$ catalysts centered at 642.5 eV and 654.0 eV. In order to determine the oxidation state of Mn and the relative ratios of Mn^{n+}, the Mn $2p_{3/2}$ spectra of catalysts are fitted into three characteristic peaks, which corresponded to Mn^{3+} (641.3 eV) and Mn^{4+} (642.1 eV), respectively [34–39]. The final peak at 644.5 eV corresponds to the satellite peak of manganese [34,37–41].

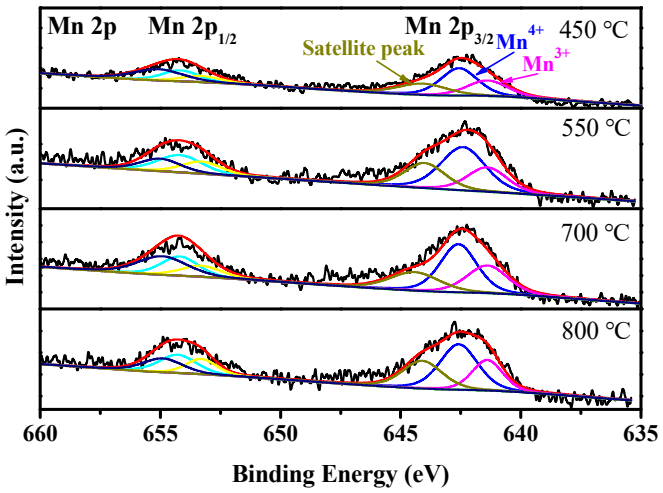

Figure 10. XPS spectra of Mn 2p over different catalysts.

From Table 3, it can be seen that the molar concentration of Mn on the surface of $MnAlO_x$-800 °C (6.033%) is much higher than that of $MnAlO_x$-700 °C (3.78%), $MnAlO_x$-550 °C (3.49%), and $MnAlO_x$-450 °C (2.227%). The relative surface content of Mn^{4+} fraction, namely, the molar ratio of $Mn^{4+}/(Mn^{4+} + Mn^{3+})$, gradually increase from 49.31% for $MnAlO_x$-450 °C to 51.36% for $MnAlO_x$-800 °C with the increase calcination temperature. It is clear that much more Mn^{4+} species are exposed on the surface of $MnAlO_x$-800 °C. It has been demonstrated that the Mn^{4+} species and their redox cycle might be beneficial for high activity in the NH_3-SCR reaction at low temperature, attributed to the enhancement of NO oxidation to NO_2 [30,35,42,43] and the subsequent facilitation of the fast-SCR reaction [30,44]. On the basis of the XPS analysis, it can be concluded that the excellent catalytic activity of $MnAlO_x$-800 °C could be attributed to the higher content of active Mn^{4+}. Meanwhile, the XPS data are consistent with the H_2-TPR analysis, and $MnAlO_x$ catalysts calcined at higher temperature are beneficial to the formation of MnO_2 phase.

2.4.3. NO Oxidation

It is reported that the enhancement of NO oxidation to NO_2 could significantly promote the catalytic activity of SCR catalysts at low temperature due to the occurrence of the fast SCR reaction: $2NH_3 + NO + NO_2 \rightarrow 2N_2 + 3H_2O$ [37,45]. Although it is mentioned that the fast SCR reaction can promote the denitration activity, this conclusion is only based on speculation. In order to more accurately determine whether a fast SCR occurred in the reaction, we further studied the process of NO oxidation to NO_2 and the results are clearly illustrated in Figure 11. With the increasing calcination temperature, the NO oxidation to NO_2 shows an obvious increase. This activity might be related to the fact that the catalyst prepared at higher calcination temperatures could provide a much more Mn^{4+}, which is beneficial to the NO oxidation reaction. Furthermore, the stronger basicity of the higher calcination temperature catalysts, which is beneficial to the adsorption of NO_x, is also the cause of the enhanced NO oxidation ability [46].

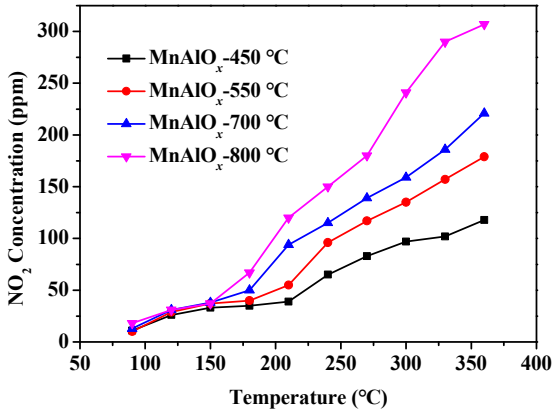

Figure 11. NO oxidation to NO_2 over the $MnAlO_x$ catalysts with different calcination temperatures. Reaction conditions: [NO] = 500 ppm, [O_2] = 6.5 vol.%, N_2 as balance gas, total gas flow rate 400 mL/min, and GHSV = 12,000 h^{-1}.

2.5. In Situ DRIFTs

2.5.1. In Situ DRIFTs of NO_x/NH_3 Adsorption

To investigate the adsorption behaviors of the NH_3/NO_x on the surface of the catalysts, the in situ DRIFTs experiments of NH_3/NO_x adsorption over the $MnAlO_x$ catalysts with different calcination temperatures are carried out, and the results are clearly presented in Figures 12 and 13.

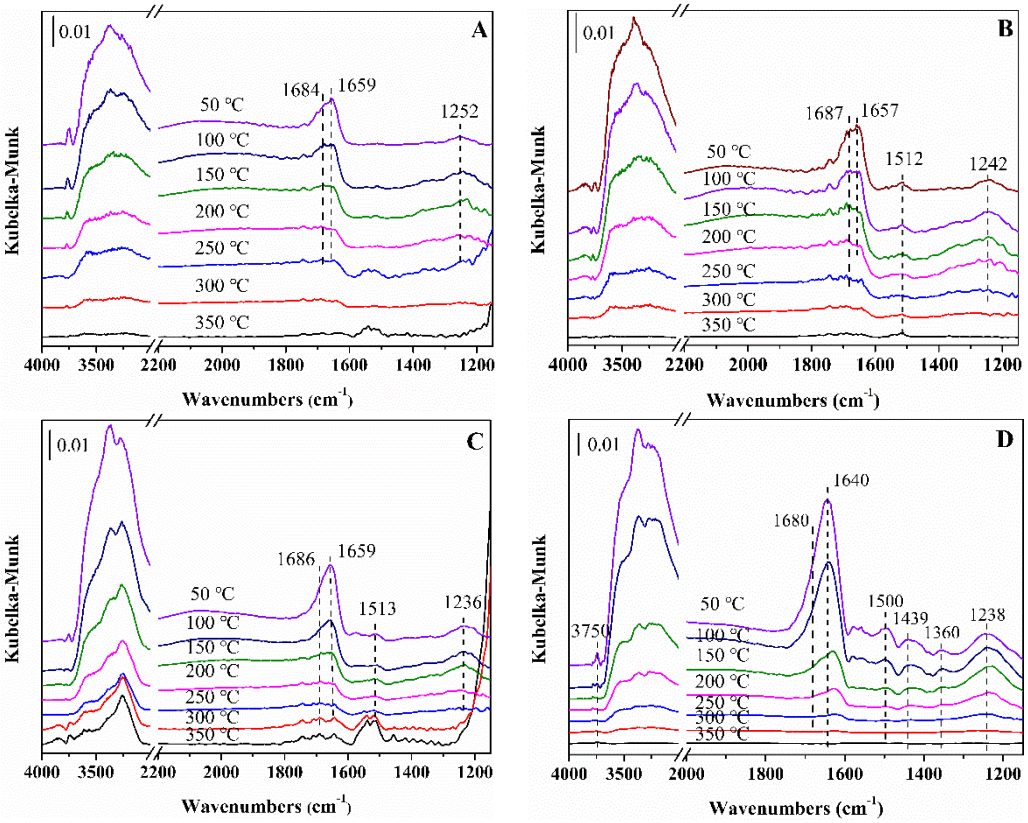

Figure 12. In situ DFIRTs of spectra of (**A**) $MnAlO_x$-450 °C, (**B**) $MnAlO_x$-550 °C, (**C**) $MnAlO_x$-700 °C, (**D**) $MnAlO_x$-800 °C catalysts under atmosphere of 500 ppm of NH_3/N_2 (100 mL/min) at 50, 100, 150, 200, 250, 300, and 350 °C.

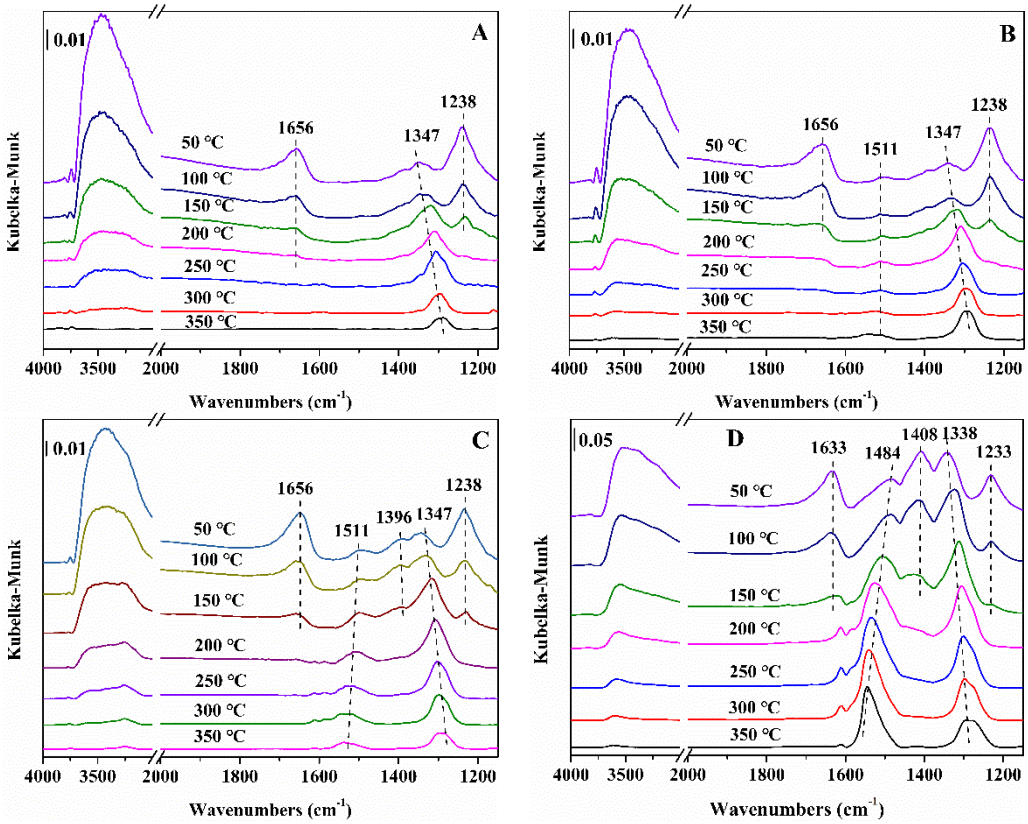

Figure 13. In situ DFIRTs of spectra of (**A**) $MnAlO_x$-450 °C, (**B**) $MnAlO_x$-550 °C, (**C**) $MnAlO_x$-700 °C, (**D**) $MnAlO_x$-800 °C catalysts under atmosphere of 500 ppm of NO + 6.5 vol. %/N_2 (100 mL/min) at 50, 100, 150, 200, 250, 300, and 350 °C.

Figure 12 displays the in situ DRIFTs spectra of $MnAlO_x$ serial catalysts after the adsorption of NH_3 at different temperature. Several bands attributed to the intermediate species of NH_3 appear at 1686, 1659, 1513, 1439, 1360, and 1242 cm^{-1}. The bands at 1686 and 1439 cm^{-1} correspond to the symmetric and asymmetric deformation vibrations of NH_4^+ ionic ($\delta_s(NH_4^+)$ and $\delta_{as}(NH_4^+)$) bound to the Brønsted acid sites [31,38,41,47–49]. The bands at 1659, 1360 and 1224 cm^{-1} are result of symmetric deformation vibration of NH_3 ($\delta_s(NH_3)$) coordinative bound to Lewis acid sites [30,38,50,51]. The bands at 1512 cm^{-1} can be assigned to the characteristic bands of amide (-NH_2) species [41,48,52,53]. In the high wavenumber region, the broad bands at 3000~3600 cm^{-1} can be ascribed to the symmetric and asymmetric stretching vibration of NH_3 ($\nu_s(NH_3)$ and $\nu_{as}(NH_3)$) coordinated to Lewis acid sites [50]. The bands at 3750 cm^{-1} could be assigned to the O-H stretching vibration modes of the surface acidic hydroxyl.

With the increase of the calcination temperature of $MnAlO_x$ catalysts, the number of peaks corresponding to adsorbed NH_3 increase, signifying that $MnAlO_x$ catalysts calcined at higher temperature could more easily activated NH_3. As the desorption temperature increase, the intensity of all bands corresponding to adsorbed NH_3 species decrease until disappear during the temperature range of 50~300 °C.

The NO + O_2 adsorption over $MnAlO_x$ catalysts at different temperature was investigated by in situ DRIFTs and the obtained spectra are shown in Figure 13, the catalysts surface is mainly covered by various types of nitrites and nitrates. The bands at 1656 cm^{-1} are assigned to the adsorbed NO_2 molecules [38,49,52]. The bands at 1511 and 1290 cm^{-1} are ascribed to chelating bidentate nitrate [49]. The bands at 1238 cm^{-1} could be assigned to bridged nitrate due to the disproportionation of NO [48]. The bands at 1408 and 1347 cm^{-1} could be ascribed to the monodentate nitrite. The bands at 1484 cm^{-1} could be assigned to the linear nitrite [36,38,54]. The bands at 3000~3700 cm^{-1} are ascribed to the stretching interaction between the surface basic hydroxyls and NO_x [47].

With the increase of the calcination temperature of $MnAlO_x$ catalysts, the number and intensity of peaks corresponding to adsorbed NH_3 increase, signifying that $MnAlO_x$ catalysts calcined at higher temperature could more easily adsorbed and activated NO_x. Adsorbed NO_2, bridged nitrate, linear nitrite, and monodentate nitrite completely vanished with the temperature up to 250 °C, and bidentate nitrates with higher thermal stability still existed as the temperature increased up to 350 °C. It is worthy noting that the band around 1486 and 1346 cm^{-1} increased at first, and afterwards decreased with the increase of temperature. With an increase in temperature to 200 °C, the bands around 1486 and 1346 cm^{-1} shifted into new bands around 1550 and 1302 cm^{-1}, respectively. These phenomena imply that NOx species could be coordinated to the surface of catalysts in the form of unstable NOx firstly, for instance, monodentate and linear nitrite. Thereafter, they were gradually oxidized into bidentate nitrates with higher thermostability, among which the active centers can be liberated. Simultaneously, NO can coordinate the released active centers to generate bidentate nitrates, giving rise to the obvious enhance in the absorbed peaks which is consistent with bidentate nitrate. Afterwards they were increasingly oxidized into bidentate nitrates, and thus lead to the distinct improvement in the absorbed peaks of bidentate nitrate. Furthermore, $MnAlO_x$ catalysts calcined at higher temperature could enhance the transformation from unstable nitrites to bidentate nitrates.

2.5.2. Adsorption of NH_3 Followed by Introduction of NO + O_2

In order to investigate the reaction pathways of NH_3 and NO reactants on $MnAlO_x$-800 °C catalysts, in situ DRIFTs spectra of the reaction between NO + O_2 and pre-adsorbed NH_3 at 210 °C as a function of time are recorded. As shown in Figure 14, the bands at 1238 cm^{-1} ascribed to $\delta_s(NH_3)$ coordinated to Lewis acid sites disappeared gradually with an increase in the exposure time of NO + O_2, which indicates that coordinated NH_3 have taken part in the SCR process. Meanwhile, the bands at 3000~3600 cm^{-1} assigned to $\nu_s(NH_3)$ and $\nu_{as}(NH_3)$ adsorbed on Lewis acid sites were gradually weakened. In addition, the bands 1662, 1550, 1473, and 1290 cm^{-1} assigned to multifarious nitrites and nitrates emerged and strengthened with increase the exposure time of NO + O_2. The Eley–Rideal (E–R) mechanism is generally considered to involve reaction between adsorbed A and gas phase B. On the basis of the above discussion, the adsorbed NH_3 species were capable of reacting with gaseous NO following E–R mechanism.

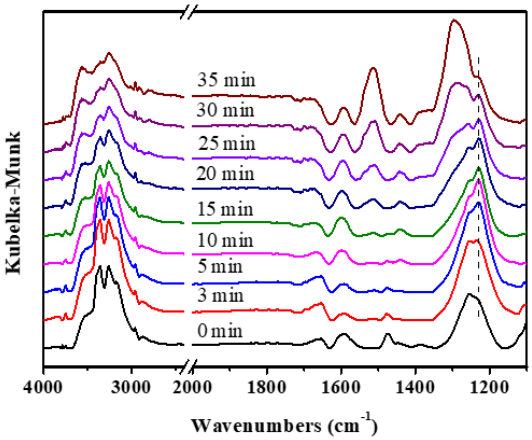

Figure 14. In situ DRIFTs spectra of the $MnAlO_x$ catalyst under an atmosphere of 500 ppm NO + 6.5 vol. %O_2/N_2 at different times after adsorption of 500 ppm of NH_3 at 210 °C and flowing of N_2 for 30 min.

2.5.3. Adsorption of NO + O_2 Followed by Introduction of NH_3

The reaction between NH_3 and pre-adsorbed NO + O_2 at 210 °C is also performed on $MnAlO_x$-800 °C catalysts by in situ DRIFTs. As shown in Figure 15, the intensity of bands at 1535 and 1292 cm^{-1} assigned to bidentate nitrate progressively decreased to some

extent with an increase in the exposure time in 500 ppm of NH_3, indicating that bidentate nitrates were the reactive species for NH_3-SCR reaction. Meanwhile, the bands at 1627 cm^{-1} attributed to adsorbed NO_2 progressively disappeared with increasing the exposure time of NH_3, suggesting that the adsorbed NO_2 were the reactive species. In addition, new bands at 3328 cm^{-1} corresponding to the stretching vibration of NH_3 adsorbed on Lewis acid sites were detected and strengthened with increasing the exposure time of NH_3. The Langmuir–Hinshelwood (L–H) mechanism is universally considered as the adsorbed A reacted with adsorbed B. Therefore, the adsorbed NO_x species were capable of reacting with coordinated NH_3 following L–H mechanism. Furthermore, the $MnAlO_x$-800 °C catalysts could enhance the transformation of nitrites to nitrates, which are the reactive intermediates and could react with NH_3, thus the $MnAlO_x$-800 °C catalysts have a higher SCR activity than that of the other $MnAlO_x$ catalysts.

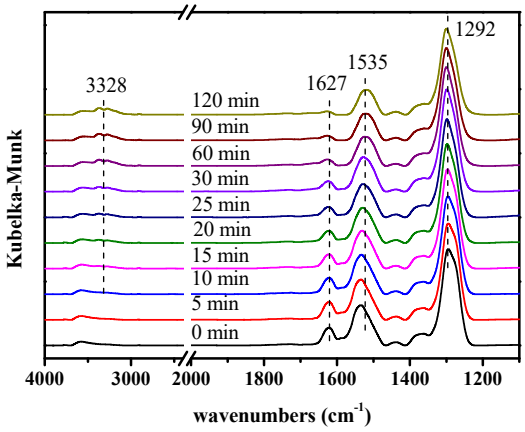

Figure 15. In situ DRIFTs spectra of the $MnAlO_x$ catalyst under an atmosphere of 500 ppm NH_3 at different times after adsorption of 500 ppm NO + 6.5 vol. $\%O_2/N_2$ of at 210 °C and flowing of N_2 for 30 min.

Hence, it could be deduced that the NH3-SCR performance on the $MnAlO_x$-800 °C samples follows both L–H and E–R mechanism. Compared to the reaction rate of adsorbed NH3 with the pre-adsorbed NO_x over the $MnAlO_x$-800 °C catalysts, the reaction rate of gas phase NO with the pre-adsorbed NH3 was rapid according to the above discussion. Hence, the E–R mechanism conducts a more dominant role.

3. Experimental

3.1. Preparation of Catalyst

Manganese alumina oxides were synthesized using a modified procedure according to those reported by Jaroniec, Yuan, and their co-workers [55,56]. The details of the synthesis processes are described in the Supporting Information (S1.1 Synthesis of Catalysts).

3.2. Characterization of the Catalysts

Thermogravimetry/differential thermogravimetry (TG/DTG) measurement was performed on a NETZSCH STA409PC (Netzsch, Selb, Germany) thermogravimetric analyzer. The TG/DTG profiles were recorded in flowing air up to 800 °C (5 °C/min heating rate).

N_2 adsorption isotherms were performed at −196 °C on Quantachrome Autosorb volumetric analyzer (Quantachrome, Boynton Beach, FL, USA). Prior to N_2 adsorption, the samples were degassed at 300 °C for 6 h under vacuum.

X-ray diffraction (XRD) was performed using D8 ADVANCE A25 (Bruker Co., Billerica, MA, USA) diffractometer with Ni-filtered Cu Kα radiation in the 2θ range from 0.4° to 5° (small angle) and from 10° to 80° (wide angle).

Energy dispersive spectroscopy (EDS) was conducted on JSM-7001F (Hitachi Limited, Tokyo, Japan) field emission scanning electron microscopy. HRTEM images was performed on a JEOL JEM 2100 transmission electron microscope(JEOL, Ltd., Tokyo, Japan).

NH_3-TPD experiments were conducted on Chemstar TPx (Quantachrome, Boynton Beach, FL, USA) apparatus. Prior to the NH_3 adsorption, the samples (100 mg) were pretreated under He flow (30 mL/min) at 350 °C for 1 h and then cooled down to 50 °C in a flow of He. Next, the catalysts were saturated with a flow of 10 vol.% NH_3/He at 50 °C for 1 h, followed by He purging for 0.5 h. After that, the furnace temperature was raised to 800 °C (10 °C/min heating rate) under He flow.

NO + O_2-TPD experiments were performed on a self-made apparatus. Prior to NO + O_2-TPD experiments, the samples (0.5 g) were pretreated under an N_2 stream (200 mL/min) at 350 °C for 1 h and then the reactor temperature was cooled to 50 °C. After that, the samples were exposed to 1000 ppm NO + 6.5% O_2 for 1 h, followed by N_2 purging for 0.5 h. Finally, the samples were heated to 600 °C (10 °C/min ramping rate) with flowing N_2 (200 mL/min). The inlet and outlet gas concentrations of NO_x were monitored by a portable FTIR gas analyzer (Gasmet Instruments DX-4000, Vantaa, Finland).

H_2-TPR experiments were performed on a Quantachrome ChemStar TPx apparatus. 100 mg of catalyst was pretreated with flowing Ar (30 mL/min) at 350 °C for 1 h. Then, the samples cooled down to 50 °C, the flowing Ar was replaced by a flow of 10.0% H_2/Ar (30 mL/min), and the furnace temperature was raised to 900 °C with a heating rate of 10 °C/min.

X-ray photoelectron spectroscopy (XPS) was conducted on a Kratos Axis Ultra DLD (Japan) multifunctional photoelectron spectrometer with Al-Kα radiation (12 kV × 15 mA, hν = 1486.6 eV) under ultrahigh vacuum. The element binding energies were calibrated by C 1s (284.8 eV).

NO oxidation experiments were performed on a custom-made apparatus. The catalysts (0.5 g) were exposed to 500 ppm NO + 6.5 vol.% O_2/N_2 (200 mL/min). The inlet and outlet gas concentration of NO_x was detected by a FTIR gas analyzer (Gasmet Instruments DX-4000, Vantaa, Finland).

The in situ DRIFTs measurements were performed on an FTIR spectrometer (Bruker Tensor 27, Germany) equipped with an MCT detector and a Harrick temperature controller. The spectra were recorded in the range of 4000~1000 cm^{-1} at a resolution of 8 cm^{-1} with 100 scans in Kubelka–Munk mode. Details are given in Supporting Information (S1.3 Characterization of Catalysts).

3.3. Catalytic Activity Measurement

The catalytic activities of $MnAlO_x$ for NH_3-SCR in excess oxygen were evaluated under atmospheric pressure in a fixed-bed continuous-flow quartz microreactor (inner diameter 12 mm). The details of the activity testing process are presented in the Supporting Information (S1.3 Catalytic Activity Measurement). The NO_x conversion and N_2 selectivity were calculated on the flowing equations [57].

$$\mathrm{NO_x\ conversion}(\%) = \left(1 - \frac{[\mathrm{NO_x}]_{\mathrm{out}}}{[\mathrm{NO_x}]_{\mathrm{in}}}\right) \times 100\%$$

$$\mathrm{N_2\ selectivity}(\%) = \left(1 - \frac{2 \times [\mathrm{N_2O}]_{\mathrm{out}}}{[\mathrm{NO_x}]_{\mathrm{in}} + [\mathrm{NH_3}]_{\mathrm{in}} - [\mathrm{NO_x}]_{\mathrm{out}} - [\mathrm{NH_3}]_{\mathrm{out}}}\right) \times 100\%$$

where the subscript indicated the inlet and outlet concentration at steady-state, respectively.

4. Conclusions

In summary, a series of mesoporous amorphous $MnAlO_x$ catalysts for NH_3-SCR at low temperature was successfully prepared. Among them, the $MnAlO_x$-800 °C catalysts exhibit the best SCR performance. The NO_x conversion of $MnAlO_x$-800 °C catalysts could

maintain above 90% at 150~240 °C and the N_2 selectivity of $MnAlO_x$-800 °C catalysts could maintain 80% up to 240 °C.

$MnAlO_x$ catalysts calcined at different temperature with uniform and ordered mesoporous structure confirmed by means of N_2-adsorption/desorption isotherms, small angle XRD, and TEM. Meanwhile, the active components MnO_x could atomic-level homogeneity distribute on the surface of $MnAlO_x$ catalysts. The $MnAlO_x$-800 °C catalysts possess improved redox properties than other $MnAlO_x$ catalysts, which is assigned to the higher content of $Mn^{4+}/(Mn^{4+} + Mn^{3+})$. In comparison with other $MnAlO_x$ catalysts, the $MnAlO_x$-800 °C catalyst has a higher adsorption ability for NO_x due to enhanced redox properties. The high adsorption ability for NO_x and improved redox properties of $MnAlO_x$-800 °C catalysts are beneficial for formation of nitrate/nitrite species on the catalyst surface to results in high SCR activity. Furthermore, the results of in situ DRIFTs indicated that adsorbed NO_2 and bidentate nitrate are the reactive intermediate species, and NH_3 species coordinated to Lewis acid sites, taking part in SCR reaction. The SCR performance followed L–H and E–R mechanism concurrently, while E–R mechanism plays a significant role.

Supplementary Materials: The following supporting information can be downloaded at: https://www.mdpi.com/article/10.3390/catal12060637/s1, Figure S1. TG-DTG curves for manganese alumina samples.

Author Contributions: Methodology, Q.H.; validation, Q.H. and Y.L.; writing—original draft preparation, Q.H.; writing—review and editing, Y.L., Y.H., X.H. and Z.H.; supervision, Y.H.; project administration, Z.H. All authors have read and agreed to the published version of the manuscript.

Funding: This research was funded by the Strategic Priority Research Program of Chinese Academy of Sciences (No. XDA29020501), the National Natural Science Foundation of China (Grants 21902173 and 21978314).

Acknowledgments: The authors gratefully acknowledge the financial support by the Strategic Priority Research Program of Chinese Academy of Sciences (No. XDA29020501), the National Natural Science Foundation of China (Grants 21902173 and 21978314).

Conflicts of Interest: The authors declare no conflict of interest.

References

1. Li, J.; Chang, H.; Ma, L.; Hao, J.; Yang, R.T. Low-temperature selective catalytic reduction of NO_x with NH_3 over metal oxide and zeolite catalysts—A review. *Catal. Today* **2011**, *175*, 147–156. [CrossRef]
2. Han, L.; Cai, S.; Gao, M.; Hasegawa, J.Y.; Wang, P.; Zhang, J.; Shi, L.; Zhang, D. Selective Catalytic Reduction of NO_x with NH_3 by Using Novel Catalysts: State of the Art and Future Prospects. *Chem. Rev.* **2019**, *119*, 10916–10976. [CrossRef] [PubMed]
3. Paolucci, C.; Khurana, I.; Parekh, A.A.; Li, S.C.; Shih, A.J.; Li, H.; Di Iorio, J.R.; Albarracin-Caballero, J.D.; Yezerets, A.; Miller, J.T.; et al. Dynamic multinuclear sites formed by mobilized copper ions in NO_x selective catalytic reduction. *Science* **2017**, *357*, 898–903. [CrossRef] [PubMed]
4. Busca, G.; Lietti, L.; Ramis, G.; Berti, F. Chemical and mechanistic aspects of the selective catalytic reduction of NO_x by ammonia over oxide catalysts: A review. *Appl. Catal. B-Environ.* **1998**, *18*, 1–36. [CrossRef]
5. Brandenberger, S.; Krocher, O.; Tissler, A.; Althoff, R. The State of the Art in Selective Catalytic Reduction of NO_x by Ammonia Using Metal-Exchanged Zeolite Catalysts. *Catal. Rev. Sci. Eng.* **2008**, *50*, 492–531. [CrossRef]
6. Boningari, T.; Smirniotis, P.G. Impact of nitrogen oxides on the environment and human health: Mn-based materials for the NO_x abatement. *Curr. Opin. Chem. Eng.* **2016**, *13*, 133–141. [CrossRef]
7. Liu, F.; Yu, Y.; He, H. Environmentally-benign catalysts for the selective catalytic reduction of NO_x from diesel engines: Structure-activity relationship and reaction mechanism aspects. *Chem. Commun.* **2014**, *50*, 8445–8463. [CrossRef]
8. Balle, P.; Geiger, B.; Kureti, S. Selective catalytic reduction of NO_x by NH_3 on Fe/HBEA zeolite catalysts in oxygen-rich exhaust. *Appl. Catal. B-Environ.* **2009**, *85*, 109–119. [CrossRef]
9. Mou, X.; Zhang, B.; Li, Y.; Yao, L.; Wei, X.; Su, D.S.; Shen, W. Rod-Shaped Fe_2O_3 as an Efficient Catalyst for the Selective Reduction of Nitrogen Oxide by Ammonia. *Angew. Chem.* **2012**, *51*, 2989–2993. [CrossRef]
10. Muñiz, J.; Marbán, G.; Fuertes, A.B. Low temperature selective catalytic reduction of NO over modified activated carbon fibres. *Appl. Catal. B-Environ.* **2000**, *27*, 27–36. [CrossRef]
11. Liu, C.; Shi, J.W.; Gao, C.; Niu, C.M. Manganese oxide-based catalysts for low-temperature selective catalytic reduction of NO_x with NH_3: A review. *Appl. Catal. A Gen.* **2016**, *522*, 54–69. [CrossRef]

12. Wallin, M.; Forser, S.; Thormählen, P.; Skoglundh, M. Screening of TiO_2-supported catalysts for selective NO_x reduction with ammonia. *Ind. Eng. Chem. Res.* **2004**, *43*, 7723–7731. [CrossRef]
13. Kijlstra, W.S.; Brands, D.S.; Poels, E.K.; Bliek, A. Mechanism of the selective catalytic reduction of NO by NH_3 over MnO_x/Al_2O_3. 1. Adsorption and desorption of the single reaction components. *J. Catal.* **1997**, *171*, 208–218. [CrossRef]
14. Kijlstra, W.S.; Brands, D.S.; Smit, H.I.; Poels, E.K.; Bliek, A. Mechanism of the selective catalytic reduction of NO by NH_3 over MnO_x/Al_2O_3. 2. Reactivity of adsorbed NH_3 and NO complexes. *J. Catal.* **1997**, *171*, 219–230. [CrossRef]
15. Ettireddy, P.R.; Ettireddy, N.; Mamedov, S.; Boolchand, P.; Smirniotis, P.G. Surface characterization studies of TiO_2 supported manganese oxide catalysts for low temperature SCR of NO with NH_3. *Appl. Catal. B-Environ.* **2007**, *76*, 123–134. [CrossRef]
16. Mu, J.; Li, X.; Sun, W.; Fan, S.; Wang, X. Enhancement of Low-Temperature Catalytic Activity over a Highly Dispersed Fe-Mn/Ti Catalyst for Selective Catalytic Reduction of NOx with NH_3. *Ind. Eng. Chem. Res.* **2018**, *57*, 10159–10169. [CrossRef]
17. Jiang, L.; Liu, Q.; Ran, G.; Kong, M.; Ren, S.; Yang, J.; Li, J. V_2O_5-modified Mn-Ce/AC catalyst with high SO_2 tolerance for low-temperature NH_3-SCR of NO. *Chem. Eng. J.* **2019**, *370*, 810–821. [CrossRef]
18. Yoshikawa, M.; Yasutake, A.; Mochida, I. Low-temperature selective catalytic reduction of NO_x by metal oxides supported on active carbon fibers. *Appl. Catal. A Gen.* **1998**, *173*, 239–245. [CrossRef]
19. Su, Y.; Fan, B.; Wang, L.; Liu, Y.; Huang, B.; Fu, M.; Chen, L.; Ye, D. MnO_x supported on carbon nanotubes by different methods for the SCR of NO with NH_3. *Catal. Today* **2013**, *201*, 115–121. [CrossRef]
20. Huang, H.Y.; Yang, R.T. Removal of NO by reversible adsorption on Fe-Mn based transition metal oxides. *Langmuir* **2001**, *17*, 4997–5003. [CrossRef]
21. Wu, Z.; Jiang, B.; Liu, Y.; Zhao, W.; Guan, B. Experimental study on a low-temperature SCR catalyst based on $MnOx/TiO_2$ prepared by sol-gel method. *J. Hazard. Mater.* **2007**, *145*, 488–494. [CrossRef] [PubMed]
22. Wu, Z.; Jiang, B.Q.; Liu, Y. Effect of transition metals addition on the catalyst of manganese/titania for low-temperature selective catalytic reduction of nitric oxide with ammonia. *Appl. Catal. B-Environ.* **2008**, *79*, 347–355. [CrossRef]
23. Jiang, B.; Liu, Y.; Wu, Z. Low-temperature selective catalytic reduction of NO on MnO_x/TiO_2 prepared by different methods. *J. Hazard. Mater.* **2009**, *162*, 1249–1254. [CrossRef] [PubMed]
24. Putluru, S.S.R.; Schill, L.; Jensen, A.D.; Siret, B.; Tabaries, F.; Fehrmann, R. Mn/TiO_2 and $Mn-Fe/TiO_2$ catalysts synthesized by deposition precipitation-promising for selective catalytic reduction of NO with NH_3 at low temperatures. *Appl. Catal. B-Environ.* **2015**, *165*, 628–635. [CrossRef]
25. Cai, W.; Yu, J.; Anand, C.; Vinu, A.; Jaroniec, M. Facile Synthesis of Ordered Mesoporous Alumina and Alumina-Supported Metal Oxides with Tailored Adsorption and Framework Properties. *Chem. Mater.* **2011**, *23*, 1147–1157. [CrossRef]
26. Sun, L.; Tian, W.; Liu, X. Magnesia-Incorporated Mesoporous Alumina with Crystalline Frameworks: A Solid Strong Base Derived from Direct Synthesis. *J. Phys. Chem. C* **2009**, *113*, 19172–19178. [CrossRef]
27. Kruk, M.; Jaroniec, M. Gas adsorption characterization of ordered organic-inorganic nanocomposite materials. *Chem. Mater.* **2001**, *13*, 3169–3183. [CrossRef]
28. Rashidi, F.; Kharat, A.N.; Rashidi, A.M.; Lima, E.; Lara, V.; Valente, J.S. Fractal Geometry Approach to Describe Mesostructured Boehmite and Gamma-Alumina Nanorods. *Eur. J. Inorg. Chem.* **2010**, *10*, 1544–1551. [CrossRef]
29. Roy, S.; Viswanath, B.; Hegde, M.S.; Madras, G. Low-temperature selective catalytic reduction of NO with NH_3 over $Ti_{0.9}M_{0.1}O_{2-\delta}$ (M = Cr, Mn, Fe, Co, Cu). *J. Phys. Chem. C* **2008**, *112*, 6002–6012. [CrossRef]
30. Liu, F.; He, H.; Ding, Y.; Zhang, C. Effect of manganese substitution on the structure and activity of iron titanate catalyst for the selective catalytic reduction of NO with NH_3. *Appl. Catal. B-Environ.* **2009**, *93*, 194–204. [CrossRef]
31. Guan, B.; Lin, H.; Zhu, L.; Tian, B.; Huang, Z. Effect of ignition temperature for combustion synthesis on the selective catalytic reduction of NOx with NH_3 over $Ti_{0.9}Ce_{0.05}V_{0.05}O_{2-\delta}$ nanocomposites catalysts prepared by solution combustion route. *Chem. Eng. J.* **2012**, *181–182*, 307–322. [CrossRef]
32. Ma, L.; Cheng, Y.S.; Cavataio, G.; McCabe, R.W.; Fu, L.X.; Li, J.H. In situ DRIFTS and temperature-programmed technology study on NH_3-SCR of NOx over Cu-SSZ-13 and Cu-SAPO-34 catalysts. *Appl. Catal. B-Environ.* **2014**, *156*, 428–437. [CrossRef]
33. Mu, W.T.; Zhu, J.; Zhang, S.; Guo, Y.Y.; Su, L.Q.; Li, X.Y.; Li, Z. Novel proposition on mechanism aspects over Fe-Mn/ZSM-5 catalyst for NH_3-SCR of NOx at low temperature: Rate and direction of multifunctional electron-transfer-bridge and in situ DRIFTs analysis. *Catal. Sci. Technol.* **2016**, *6*, 7532–7548. [CrossRef]
34. Thirupathi, B.; Smirniotis, P.G. Co-doping a metal (Cr, Fe, Co, Ni, Cu, Zn, Ce, and Zr) on Mn/TiO_2 catalyst and its effect on the selective reduction of NO with NH_3 at low-temperatures. *Appl. Catal. B-Environ.* **2011**, *110*, 195–206. [CrossRef]
35. Thirupathi, B.; Smirniotis, P.G. Nickel-doped Mn/TiO_2 as an efficient catalyst for the low-temperature SCR of NO with NH_3: Catalytic evaluation and characterizations. *J. Catal.* **2012**, *288*, 74–83. [CrossRef]
36. Meng, D.; Zhan, W.; Guo, Y.; Guo, Y.; Wang, L.; Lu, G. A Highly Effective Catalyst of Sm-MnO_x for the NH_3-SCR of NO_x at Low Temperature: Promotional Role of Sm and Its Catalytic Performance. *ACS Catal.* **2015**, *5*, 5973–5983. [CrossRef]
37. Chen, J.; Shen, M.; Wang, X.; Qi, G.; Wang, J.; Li, W. The influence of nonstoichiometry on $LaMnO_3$ perovskite for catalytic NO oxidation. *Appl. Catal. B-Environ.* **2013**, *134*, 251–257. [CrossRef]
38. Wang, B.; Wang, M.; Han, L.; Hou, Y.; Bao, W.; Zhang, C.; Feng, G.; Chang, L.; Huang, Z.; Wang, J. Improved Activity and SO_2 Resistance by Sm-Modulated Redox of $MnCeSmTiO_x$ Mesoporous Amorphous Oxides for Low-Temperature NH_3-SCR of NO. *ACS Catal.* **2020**, *10*, 9034–9045. [CrossRef]

39. Xu, Q.; Fang, Z.; Chen, Y.; Guo, Y.; Guo, Y.; Wang, L.; Wang, Y.; Zhang, J.; Zhan, W. Titania-Samarium-Manganese Composite Oxide for the Low-Temperature Selective Catalytic Reduction of NO with NH_3. *Environ. Sci. Technol.* **2020**, *54*, 2530–2538. [CrossRef]
40. Xiong, S.; Xiao, X.; Huang, N.; Dang, H.; Liao, Y.; Zou, S.; Yang, S. Elemental Mercury Oxidation over Fe-Ti-Mn Spinel: Performance, Mechanism, and Reaction Kinetics. *Environ. Sci. Technol.* **2017**, *51*, 531–539. [CrossRef]
41. Yang, G.; Zhao, H.; Luo, X.; Shi, K.; Zhao, H.; Wang, W.; Chen, Q.; Fan, H.; Wu, T. Promotion effect and mechanism of the addition of Mo on the enhanced low temperature SCR of NO_x by NH_3 over MnO_x/γ-Al_2O_3 catalysts. *Appl. Catal. B-Environ.* **2019**, *245*, 743–752. [CrossRef]
42. Zhang, D.; Zhang, L.; Shi, L.; Fang, C.; Li, H.; Gao, R.; Huang, L.; Zhang, J. In situ supported MnO_x-CeO_x on carbon nanotubes for the low-temperature selective catalytic reduction of NO with NH_3. *Nanoscale* **2013**, *5*, 1127–1136. [CrossRef] [PubMed]
43. Fang, C.; Zhang, D.S.; Cai, S.X.; Zhang, L.; Huang, L.; Li, H.R.; Maitarad, P.; Shi, L.; Gao, R.; Zhang, J. Low-temperature selective catalytic reduction of NO with NH_3 over nanoflaky MnO_x on carbon nanotubes in situ prepared via a chemical bath deposition route. *Nanoscale* **2013**, *5*, 9199–9207. [CrossRef] [PubMed]
44. Shan, W.; Liu, F.; He, H.; Shi, X.; Zhang, C. Novel cerium-tungsten mixed oxide catalyst for the selective catalytic reduction of NO_x with NH_3. *Chem. Commun.* **2011**, *47*, 8046–8048. [CrossRef] [PubMed]
45. Yang, S.; Wang, C.; Li, J.; Yan, N.; Ma, L.; Chang, H. Low temperature selective catalytic reduction of NO with NH_3 over Mn–Fe spinel: Performance, mechanism and kinetic study. *Appl. Catal. B-Environ.* **2011**, *110*, 71–80. [CrossRef]
46. Qi, G.; Yang, R.T. A superior catalyst for low-temperature NO reduction with NH_3. *Chem. Commun.* **2003**, 848–849. [CrossRef]
47. Pena, D.A.; Uphade, B.S.; Reddy, E.P.; Smirniotis, P.G. Identification of surface species on titania-supported manganese, chromium, and copper oxide low-temperature SCR catalysts. *J. Phys. Chem. B* **2004**, *108*, 9927–9936. [CrossRef]
48. Wu, Z.; Jiang, B.; Liu, Y.; Wang, H.; Jin, R. DRIFT Study of Manganese/Titania-Based Catalysts for Low-Temperature Selective Catalytic Reduction of NO with NH_3. *Environ. Sci. Technol.* **2007**, *41*, 5812. [CrossRef]
49. Chen, L.A.; Li, J.; Ge, M. DRIFT Study on Cerium−Tungsten/Titiania Catalyst for Selective Catalytic Reduction of NO_x with NH_3. *Environ. Sci. Technol.* **2010**, *44*, 9590–9596. [CrossRef]
50. Lin, C.-H.; Bai, H. Surface acidity over vanadia/titania catalyst in the selective catalytic reduction for NO removal—in situ DRIFTS study. *Appl. Catal. B Environ.* **2003**, *42*, 279–287. [CrossRef]
51. Zhang, L.; Shi, L.; Huang, L.; Zhang, J.; Gao, R.; Zhang, D. Rational Design of High-Performance $DeNO_x$ Catalysts Based on $Mn_xCo_{3-x}O_4$ Nanocages Derived from Metal–Organic Frameworks. *ACS Catal.* **2014**, *4*, 1753–1763. [CrossRef]
52. Qi, G.S.; Yang, R.T.; Chang, R. MnO_x-CeO_2 mixed oxides prepared by co-precipitation for selective catalytic reduction of NO with NH_3 at low temperatures. *Appl. Catal. B-Environ.* **2004**, *51*, 93–106. [CrossRef]
53. Liu, Z.M.; Zhang, S.X.; Li, J.H.; Ma, L.L. Promoting effect of MoO_3 on the NOx reduction by NH_3 over CeO_2/TiO_2 catalyst studied with in situ DRIFTS. *Appl. Catal. B-Environ.* **2014**, *144*, 90–95. [CrossRef]
54. Xin, Y.; Li, H.; Zhang, N.; Li, Q.; Zhang, Z.; Cao, X.; Hu, P.; Zheng, L.; Anderson, J.A. Molecular-Level Insight into Selective Catalytic Reduction of NO_x with NH_3 to N_2 over a Highly Efficient Bifunctional V_a-MnO_x Catalyst at Low Temperature. *ACS Catal.* **2018**, *8*, 4937–4949. [CrossRef]
55. Yuan, Q.; Yin, A.; Luo, C.; Sun, L.; Zhang, Y.; Duan, W.; Liu, H.; Yan, C. Facile synthesis for ordered mesoporous gamma-aluminas with high thermal stability. *J. Am. Chem. Soc.* **2008**, *130*, 3465–3472. [CrossRef]
56. Morris, S.M.; Fulvio, P.F.; Jaroniec, M. Ordered Mesoporous Alumina-Supported Metal Oxides. *J. Am. Chem. Soc.* **2008**, *130*, 15210–15216. [CrossRef]
57. Wang, P.L.; Gao, S.; Wang, H.Q.; Chen, S.; Chen, X.B.; Wu, Z.B. Enhanced dual resistance to alkali metal and phosphate poisoning: Mo modifying vanadium-titanate nanotubes SCR catalyst. *Appl. Catal. A Gen.* **2018**, *561*, 68–77. [CrossRef]